Case Report **IJCR (2021) 5:202**

International Journal of Case Reports (ISSN:2572-8776)

Seckel Syndrome & Skull Morphology: Quantifying Characteristics

Steven A. Lewis*, Stuart Inglis, PhD, Scott Doyle, PhD

Department of Pathology & Anatomical Sciences, University at Buffalo 955 Main St., Buffalo, NY 14203

ABSTRACT

Seckel Syndrome is a rare genetic disorder which causes morphological changes throughout the body. Some of the most commonly reported changes are those present within the cranium and mandible such as microcephaly, a beak-like nose with convex nasal ridge, and mandibular deformities such as micrognathia. However, these clinical terms provide insufficient information to allow for proper diagnosis or to understand the distortions in physiology that take place with the disease. Therefore, quantification of the features of the skull are necessary to further explain this pathology, and comparisons to normal variation will help to understand the degree to which the anatomy is affected. Seckel Syndrome is classified as a member of the microcephaly family of pathologies; however, our results demonstrate that the overall volume of the skull is not as significantly decreased as the cranial vault itself, which may provide the catalyst for Chiari Type I malformations. The mandible, likewise, is severely altered by Seckel Syndrome decreases in approximately 44% of its volume and demonstrating altered physical proportions. Finally, the osteological measurements of the facial features demonstrated inconsistent findings between different anatomical structures providing evidence that Seckel Syndrome may have a variable effect on the different bones and tissues of the skull.

Keywords: Seckel Syndrome; Skull Morphology; Microcephaly; Computational Biology; CT; Morphometrics

***Correspondence to Author:**
Steven Lewis
716-393-8038, fax: 716-829-2725,
Address: 955 Main St. Room 4212, Buffalo, NY 14203

How to cite this article:
Steven A. Lewis, Stuart Inglis, Scott Doyle. Seckel Syndrome & Skull Morphology: Quantifying C-haracteristics. International Journal of Case Reports, 2021; 5:202.

eSciPub LLC, Houston, TX USA.
Website: http://escipub.com/

INTRODUCTION

Seckel syndrome (SCKL) is a very rare genetic disorder caused by mutations leading to aberrant DNA repair function, and mitotic cellular architecture (O'Driscoll, et al. 2003, Seckel syndrome 2015). According to the Genetic and Rare Diseases Information Centre, eight subtypes of SCKL exist as a result of the eight currently known mutations in DNA repair genes ranging from ataxia-telangiectasia and Rad3-related proteins, to multiple DNA endonuclease enzymes such as RBBP8, and centromere architectural proteins such as Ninein. Many of these subtypes were originally associated with another disease known as autosomal recessive primary microcephaly (MCPH), but as a result of further research, MCPH and SCKL were combined into a spectrum disorder (MCPH-SCKL) (Seckel syndrome 2015). The overall result of this protein dysfunction leads to an accumulation of double-stranded DNA breaks which cause the symptomology of MCPH-SCKL (O'Driscoll, et al. 2004).

Some of MCPH-SCKL's most common features are: microcephaly, stunted growth both pre-natal and post-natal, cognitive deficits, dwarfism, craniosynostosis, narrow face and convex nasal ridge contributing to a "beak-like" appearance, and cachexia (Seckel syndrome 2015). As a result of these craniofacial and developmental symptoms, MCPH-SCKL has been also referred to as bird-nosed/faced dwarfism. In addition to these features, multiple cases have reported oral malformations such as micrognathia, and other dental deformities such as oligodentia, dental overcrowding, and impacted teeth (DeCoster, et al. 2005, Regen, Nelson and Woo 2010) such as those present in **Figure 1**.

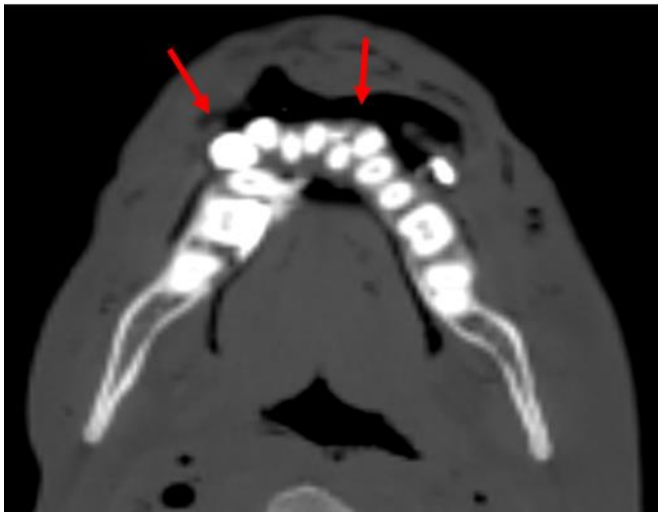

Figure 1: CT image of the MCPH-SCKL cadaver.
The red arrows indicate malocclusion sites within the mandible.

Other microcephallic disorders such as microcephallic osteodyplastic primordial dwarfism (MOPD) display very similar phenotypes to MCPH-SCKL, and as a result, strict definitions based on the severity of mental and growth retardation, as well as the presence of osteological malformations are required for diagnostic criteria (Majewski and Goecke 1982). Thus, the anatomical differences are an important feature in accurately identifying the disease phenotype and further understanding the disease progression and physiological characteristics.

Computational Morphometrics

Quantification of physical characteristics in disease and variability is an important part of understanding clinically relevant features. With the advent of modern day biomedical imaging, it is possible to perform more robust shape quantification, instead of the limitations of physical measurements, and to generate reproducible results based on proven algorithms without the need to preserve the physical material for extensive periods of time. In addition, with computational methods, comparative analysis of structures

between specimens, diseases, and anatomically normal samples is possible, expanding upon the understanding of the structure of interest and the morphological impact of disease.

To our knowledge, only one study has been performed to quantify these phenotypic differences in SCKL. In Kjaer, *et al* 2000, x-ray radiography was used to evaluate the morphology of 4 siblings, 2 boys and 2 girls, with SCKL (Kjaer, et al. 2001). In this study, the clinician used the physical radiograph and pencil to measure landmark points and distances for analysis. As a result of this study, some measurements of patients with SCKL are known, but the results are limited due to the 2D nature of the dataset, and biased by the manual measurements. Our goal is to quantify some of the morphological differences resulting from MCPH-SCKL on the cranium and mandible. Our hypothesis is that there will be significant quantitative differences between a patient with MCPH-SCKL compared to cadaveric samples with normal variation and that some of these features will provide clinically relevant aspects of the disease.

MATERIALS & METHODS

Thanks to the charitable donations from the University at Buffalo Anatomical Gift Program, eleven male cadaveric specimens underwent whole-body, hi-res, non-contrast enhanced CT imaging using a GE Discovery 690 helical CT with a tube current of 99 mA, an exposure time of approximately 1800 seconds per cadaver, and an 11 point lung convolution kernel. The voxel dimensions were 1.117mm X 1.117mm X 1.25mm. One Caucasian specimen was verified as a MCPH-SCKL patient from his private clinician and was approximately 30 years old. The other ten specimens were aged 50 or older and consisted of all Caucasian individuals and were used to represent a sampling of normal development (henceforth, referred to as the sample population). All presented cadavers underwent traditional formalin fixation.

Segmentation of the cranium and mandible was performed using the platform 3D Slicer (3D Slicer n.d., Kikinis, Pieper and Vosburgh 2014, Fredorov, et al. 2012). The images were thresholded at 100 Hounsfield units (HU) to isolate bone, and manually cleaned to separate the mandible from the cranium (Figure 2a-d).

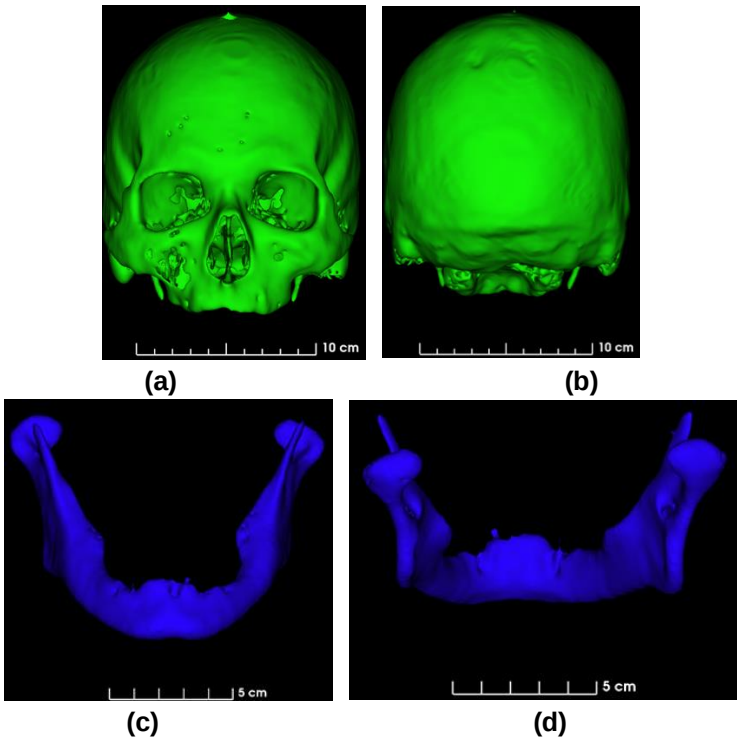

Figure 2: An example of the primary segmentations created from the skull.
(a) The cranium segmentation along the anterior view.
(b) The cranium segmentation along the posterior side.
(c) The mandible along the anterior view. (d) The posterior side of the mandible.

In addition, the mandible and maxilla were cleaned to remove the dentition and alveolar bone to prevent metric distortions based off from the presence or absence of these in the specimens. Shape measurements were taken using the virtual rulers and the SlicerRadiomics (SR) module (Joost, et al. 2017). Specifically, SR was used to compute the 3D shape characteristics: volume, sphericity, surface area, elongation, maximum 3D diameter, major axis length, and least axis length. 2D measurements were taken using the 3D Slicer rulers and consisted of: the length and width of the foramen magnum, the anterior and posterior distance from atlas to the cranium, the major and minor axes of the orbit, the length of the zygomatic process, the distance between rhinion and akanthion, and the largest horizontal distance of the nasal cavity, the distance between the mandibular angles, the distance between the mandibular condyles, and the distance between the left and right mandibular angles to the mental protuberance.*

RESULTS

Quantifying Microcephaly

Microcephaly is a principal component to diagnosing MCPH-SCKL and defining the relationship between MCPH-SCKL and other dwarfisms. The set of 3D features listed above quantified this aspect of MCPH-SCKL. Table 1 summarizes these findings, with asterisks indicating the deviation of the MCPH-SCKL sample from the average measurements of the sample population.

Table 1: 3D volumetric analysis of the cranium.
Each asterisk indicates a distance of greater than one standard deviation away from the average, while **** indicates a distance of greater than four or more standard deviations away from the average.

Impact of Seckel Syndrome on The Cranium					
Metric:	Mean ± STD:	Median:	Interquartile Range:	Seckel Syndrome:	Significance:
Volume of the Cranium (mm^3)	570014.74 ± 100654.59	550473.15	70438.59	373496.30	**
Surface to Volume Ratio of Cranium (1/mm)	0.47 ± 0.06	0.49	0.11	0.49	
Maximum 3D Diameter of Cranium (mm)	215.42 ± 7.48	214.92	10.96	196.18	***
Major Axis Length of Cranium (mm)	206.08 ± 10.29	206.83	14.19	186.10	*
Least Axis Length of Cranium (mm)	156.66 ± 5.87	158.45	6.79	128.44	****
Sphericity of Cranium	0.13 ± 0.01	0.12	0.02	0.14	
Flatness of Cranium	0.76 ± 0.04	0.74	0.05	0.69	**
Elongation of Ellipsoid of Cranium	0.87 ± 0.05	0.85	0.05	0.86	

* The equations for calculating the 3D features can be found within the documentation for the Python Radiomics package online at https://pyradiomics.readthedocs.io/en/latest/index.html (van Griethuysen, *et al.* 2017).

Further examination of the volume of the craniums is shown in figure 3 with the average and standard error plotted in comparison to MCPH-SCKL. In addition, figure 4 illustrates the average flatness of the sample population when compared to the MCPH-SCKL sample.

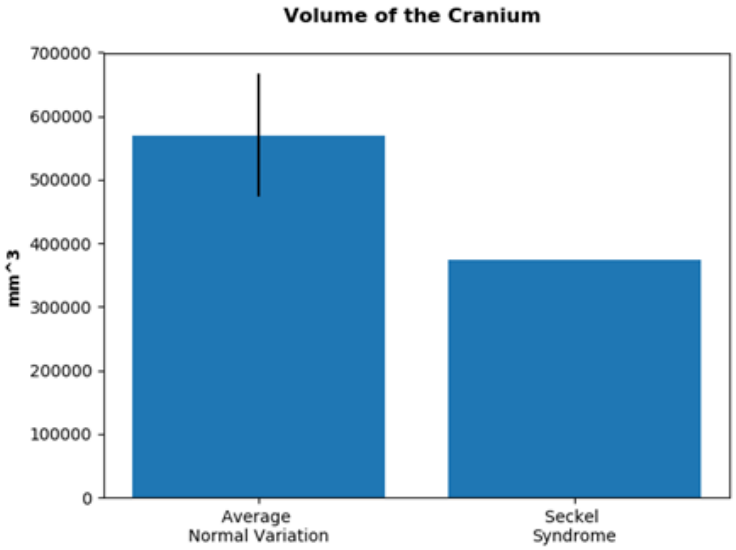

Figure 3: The average volume of the cranium from N=10 sample population specimens compared to the MCPH-SCKL sample. The standard deviation is shown for the average.

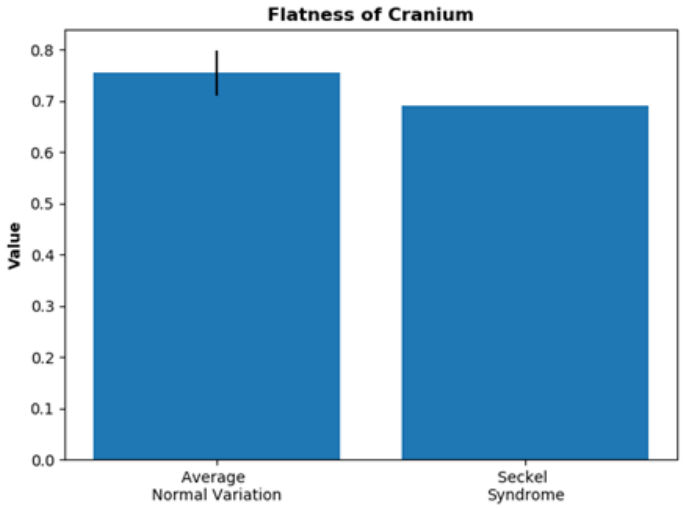

Figure 4: The mean flatness of the cranium from N=10 sample population specimens compared to the MCPH-SCKL specimen. The standard deviation is shown for the average.

The volume of the cranium in MCPH-SCKL was shown to be roughly 36.7% smaller than the sample population while the maximum 3D diameter and major axis length of MCPH-SCKL were reduced in the Seckel sample by 8.9-9.9% (approximately 20 mm) from the sample population average. The least axis length of MCPH-SCKL decreased by 18.02% (30.8 mm) from the sample population average.

Impact on the Cranial Vault, Foramen Magnum & Atlas

The cranial vault was segmented from the cranial models using manual segmentation to evaluate the possible impact of osteological features of MCPH-SCKL on the brain. For example, Chiari Type I malformations which have been reported in MCPH-SCKL due to the craniosynastosis and microcephaly (Hopkins and Haines 2003). Figure 5a shows an example of this segmentation within the cranium.

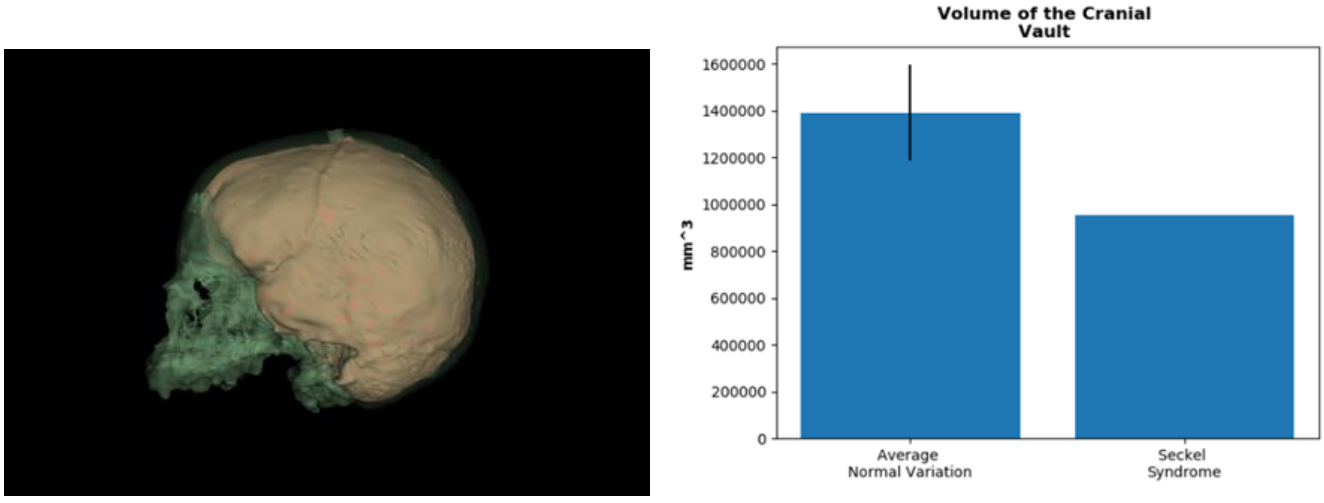

(a) **(b)**

Figure 5: MCPH-SCKL impact on cranial vault volume.
(a) An image depicting the volume of the cranial vault computed within the cranium segmentation.
(b) The mean volume of the cranial vault from N=10 sample population compared to the MCPH-SCKL sample. The standard deviation is shown for the average.

Table 2: 3D volumetric analysis of the cranial vault and the impact of MCPH-SCKL on the base of the skull. Each asterisk indicates a distance of greater than one standard deviation away from the average, while **** indicates a distance of greater than four or more standard deviations away from the average.

Impacts of Microcephaly on the Cranial Vault, Foramen Magnum & Atlas					
Metric:	Mean ± STD:	Median:	Interquartile Range:	Seckel Syndrom:	Significance:
Volume of the Cranial Vault (mm^3)	1435097.64 ± 165303.30	1490046.69	217778.44	951856.91	**
Maximum 3D Diameter of Cranial Vault (mm)	175.17 ± 10.48	173.19	13.70	156.77	*
Major Axis Length of Cranial Vault (mm)	152.95 ± 9.59	153.90	14.19	134.63	*
Least Axis of Cranial Vault (mm)	109.25 ± 4.79	110.77	6.24	98.33	**
Elongation of Ellipsoid of Cranial Vault (mm)	0.81 ± 0.05	0.80	0.07	0.77	
Sphericity of Cranial Vault	0.79 ± 0.04	0.80	0.02	0.64	***
2D Elongation of Foramen Magnum	0.85 ± 0.09	0.85	0.14	0.85	
Average Distance Between Atlas & Cranium (mm)	9.85 ± 1.54	10.03	2.72	3.48	****

3D features were used to evaluate MCPH-SCKL's effects on the cranial vault (Table 2). The volume of the cranial vault in the MCPH-SCKL patient was observed to decrease by 33.67% from the sample population average. To illustrate this, figure 5b shows the average volume and standard error for the sample population compared to MCPH-SCKL. The maximum 3D diameter, major axis length, and least axis length of the cranial vault in MCPH-SCKL all decreased by approximately 12-14% from the sample population average.

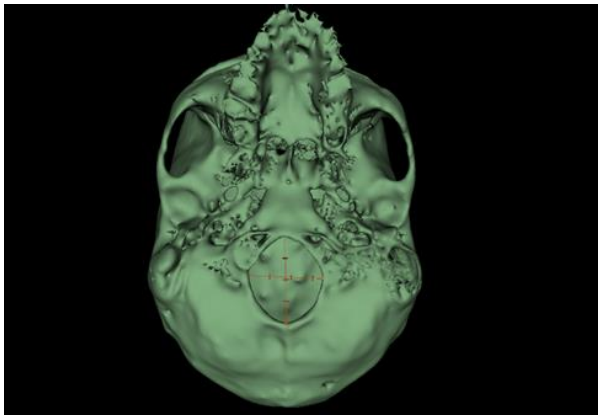

Figure 6: An image depicting the major and minor axes defined for the 2D elongation calculations of the foramen magnum.

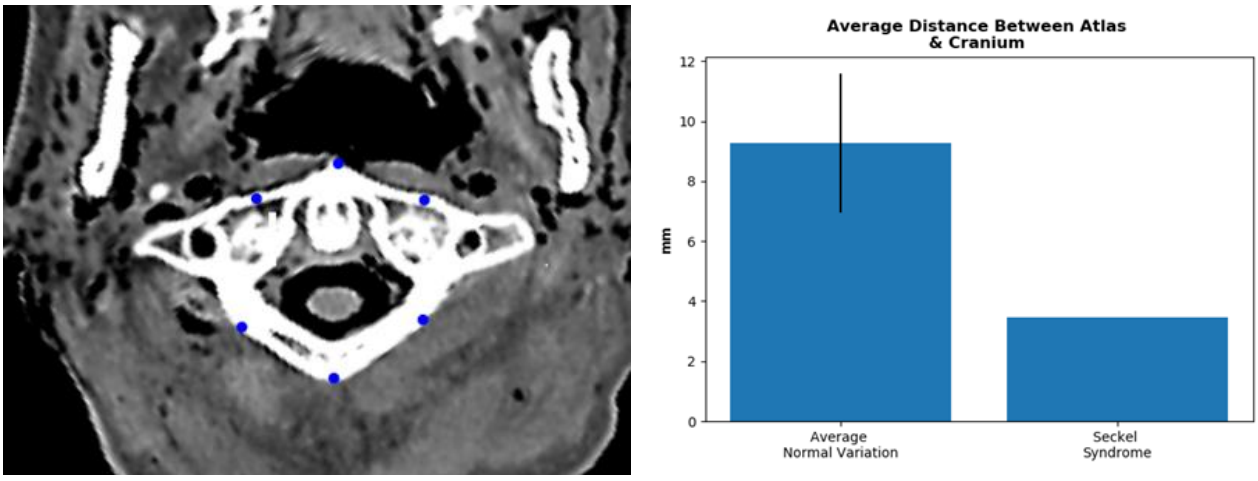

(a) **(b)**

Figure 7: The distance between atlas and the cranium.
(a) An image depicting the three anterior and three posterior points along the lateral surface of atlas used to measure the distance between atlas and the cranium for each sample.
(b) The calculated average distance between atlas and cranium for N=10 samples compared to the MCPH-SCKL specimen. The standard deviation is shown for the average.

To evaluate the effects of MCPH-SCKL on the base of the skull and its orientation to atlas, 2D analysis was performed. The major and minor axes lengths of the foramen magnum were measured using the 3D Slicer rulers and used to calculate the elongation of the foramen magnum (Figure 6). In addition, 3 anterior points of atlas and 3 posterior points of atlas were used to calculate the average distance between atlas and the nearest point on the skull (Figure 7a). These values are also reported within table 2. The average distance between atlas and the cranium in MCPH-SCKL decreased from the sample population average by 5.6 mm or 64.71%. Figure 7b illustrates the average distances for the sample population compared to the MCPH-SCKL specimen.

Quantifying Facial Morphology

Distinct facial feature morphology is another reported phenomenon in MCPH-SCKL patients.

MCPH-SCKL has been referred to as bird-nosed dwarfism due to these significant facial deformation presented in patients such as the beak-like nose, narrow face, and convex nasal ridge (Kjaer, et al. 2001, Seckel syndrome 2015). To evaluate some of these features and the impact of developmental and morphological distortions from the skull, the orbit, zygomatic processes, and nasal cavity were analyzed. The major and minor axes were defined and measured for length (figure 8).

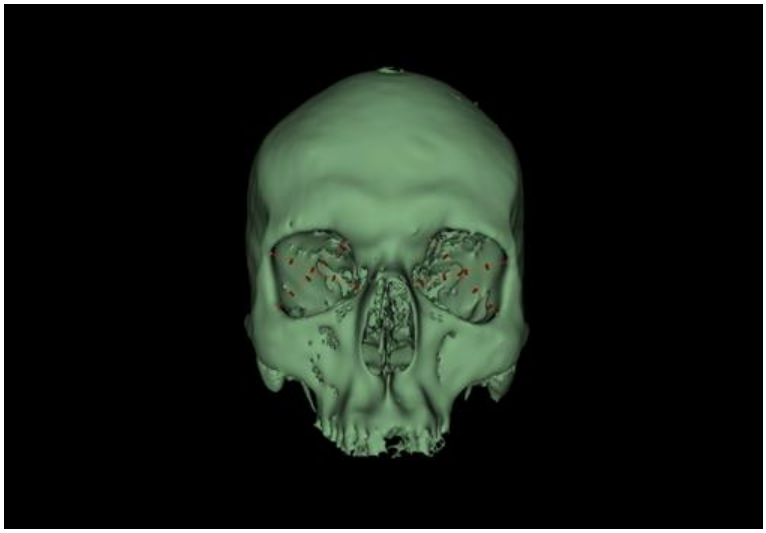

Figure 8: An image depicting the major and minor axes of the orbit used to compute the average 2D elongation of the orbit for each sample.

The average length of both the major and minor axes for the orbit was decreased by 23%. Elongation was then calculated from these values and compared between the samples and MCPH-SCKL.

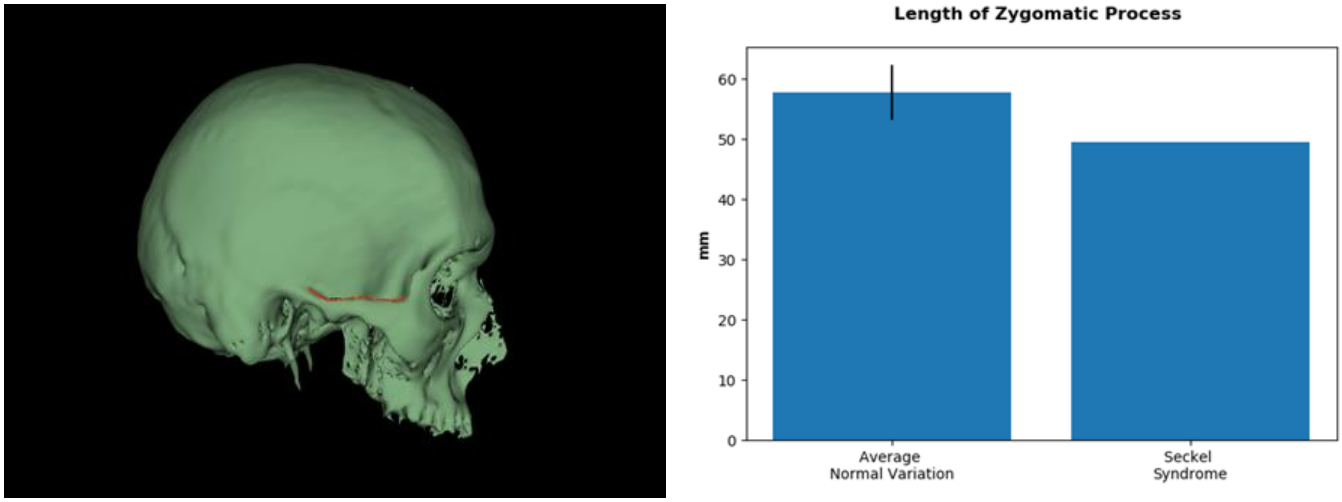

(a) **(b)**

Figure 9: Deformations of the cheekbones.
(a) A representation of the length measurement along the superior surface of the zygomatic process. (b) The calculated average length of the right and left zygomatic processes between N=10 sample population specimens and the MCPH-SCKL sample. The standard deviation is shown for the average.

To evaluate the zygomatic arches multiple rulers were used to determine the superior length for each arch and averaged (figure 9a). The average of these values for the sample population was compared to the MCPH-SCKL sample in figure 9b illustrating a decrease of approximately 15.36% in the MCPH-SCKL sample from the sample population mean.

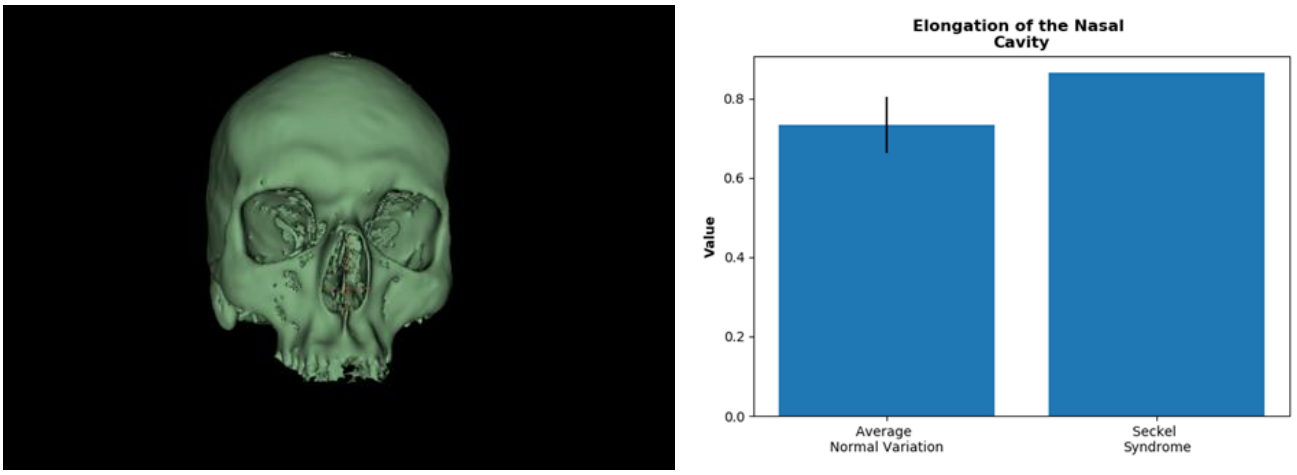

(a) **(b)**

Figure 10: Deformations of the nasal cavity.
(a) A representation of the distance between rhinion to akanthion, and the largest lateral distance of the nasal cavity. (b) The calculated average elongation of the nasal cavity for N=10 sample population specimens compared to the MCPH-SCKL sample. The standard deviation is shown for the average.

Finally, to evaluate the nasal cavity, the distance between rhinion and akanthion was used along with the maximum lateral distance of the nasal cavity (figure 10a). These values were then used to calculate elongation of the nasal cavity and compared between samples (figure 10b). A summary of these results is presented in table 3.

Table 3: Landmark analysis of facial attributes. Each asterisk indicates a distance of greater than one standard deviation away from the average, while **** indicates a distance of greater than for or more standard deviations away from the average.

Impacts of Microcephaly on Facial Morphology					
Metric:	Mean ± STD:	Median:	Interquartile Range:	Seckel Syndrome:	Signifi-cance:
2D Elongation of Orbit	0.95 ± 0.05	0.96	0.04	0.96	
Length of Zygomatic Process (mm)	58.54 ± 4.10	56.90	4.26	49.55	**
2D Elongation of the Nasal Cavity	0.72 ± 0.06	0.73	0.06	0.86	**

Quantifying Micrognathia

MCPH-SCKL patients have been reported to display extreme defects in dentition and the mandible (DeCoster, et al. 2015, Kjaer, et al. 2001, and Regen, Nelson and Woo 2010). As illustrated in figure 1, the MCPH-SCKL cadaver also presented with dental malocclusions, including dental overcrowding and impacted teeth. To try to understand the impact of this and other aspects of MCPH-SCKL on the mandible, shape characteristics were first computed including the volume, maximum 3D diameter, major axis length and least axis length (table 4). The MCPH-SCKL patient had and reduction in mandibular volume by 41.13%. The maximum 3D diameter, major axis length, and least axis length were all reduced by 18-28% in MCPH-SCKL from the sample population average.

Table 4: 3D volumetric analysis of the mandible, and landmark analysis of mandibular aspects. Each asterisk indicates a distance of greater than one standard deviation away from the average, while **** indicates a distance of greater than for or more standard deviations away from the average.

Impact of Seckel Syndrome on the Mandible					
Metric:	Mean ± STD:	Median:	Interquartile Range:	Seckel Syndrome:	Significance:
Volume of Mandible (mm^3)	19759.94 ± 7391.53	52105.76	7540.14	29289.34	**
Maximum 3D Diameter of Mandible (mm)	133.56 ± 6.35	133.03	10.40	102.02	****
Major Axis Length of Mandible (mm)	138.31 ± 9.18	135.23	14.41	98.88	****
Least Axis Length of Mandible (mm)	38.42 ± 4.69	38.22	7.87	31.42	*
Distance Between Mandibular Angles (mm)	91.05 ± 3.82	90.20	5.35	73.60	****
Distance Between Mandibular Condyles (mm)	103.03 ± 7.68	103.55	10.85	79.90	***
Average Distance Between Mandibular Angles & Mental Protuberance (mm)	85.12 ± 5.07	85.43	4.64	66.20	***

Finally, the distance between the mandibular condyles, mandibular angles, and the average distance between the mandibular angles and the mental protuberance were calculated. A summary of all mandibular condyle measurements can be found in table 4. The mandibular condyles decreased in MCPH-SCKL compared to the sample population mean in distance by 27 mm, while the mandibular angles decreased by 18.7 mm, and the average distance between the mandibular angles and the mental protuberance decreased by 21.2 mm. This is a 24-25% decrease in the distance between the condyles and the angles to the mental protuberance, and a 20% decrease in distance between the mandibular angles.

DISCUSSION

Through the use of modern medical imaging and analytical tools, morphological diseases can be described through quantitative results rather than through qualitative descriptions. Microcephaly has been reported as a prominent feature in MCPH-SCKL in the past. However, our results have shown that, while cranial size does decrease (table 1 and figure 3), the more significant decrease is observed in the cranial vault volume (table 2 and figure 5b) which may demonstrate a stronger connection between

craniosynastosis and MCPH-SCKL effects on the brain. Although the MCPH-SCKL patient did not have a hisotry of Chiari Type I malformation, these findings could explain why these malformations have been found in the past.

As expected, all of the calculated 3D shape distances including the maximum 3D diameter, major axis length, and least axis length were substantially decreased in the cranium, cranial vault, and mandible providing more support for the developmental constraints in MCPH-SCKL (tables 1-3). However, the most interesting measurement from the cranium was the least axis length which represents the measurement of the smallest axis created when an ROI is enclosed within an ellipsoid. While the least axis length of the cranium was drastically reduced within MCPH-SCKL, the elongation of the ellipsoid (which was measured using the least axis and major axis length) was not significantly different (table 1). This indicates a flattening of the cranium in MCPH-SCKL which is supported by the flatness values calculated (table 1 and figure 4). Further evidence of this can be seen in the impacts on the cranial vault, as the least axis length is more drastically impacted than the major axis length, but the cranial vault is not as significantly flattened as the cranium due to the lack of attachments such as the facial bones which elongate the cranium (table 2).

When looking at the sphericity of the cranium and the cranial vault, however, these shape features were not drastically impacted by MCPH-SCKL (table 1 & 2). Sphericity is a calculation towards the roundness of an object, where spherical objects generate values at or close to one, and flat objects would generate values at or close to 0. However, sphericity takes into account the entire surface area and volume, thus the results might be skewed due to the equation compensating for shape deformations in certain regions of the model based off from the rest of the model attributes. The positioning of the least axis in the cranial vault and the cranium lies in the coronal plane of the body, which may indicate that the superior coronal, metopic, and sagittal sutures may have fused earlier on that the posterior and lateral lamboid and the squamous sutures providing more flexibility in growth along the transverse plane.

Due to the commonality in Chiari Type I malformations and the drastic effects from constraining the cranial vault, it was expected that there would be some distortion in the structure of the formamen magnum. However, the 2D elongation of the formamen magnum was not significant (table 2 and figure 6). Interestingly, the average distance between atlas and the foramen magnum was significantly diminished in the MCPH-SCKL sample (table 2, figures 7a,b). This could indicate a clinically significant developmental defect, or it could signify damage to the ligaments supporting the skull with atlas that cause the skull to decend. In addition, this could indicate a significant amount of fluid buildup or hydrated tissue between atlas and the cranium, which decreased more intensely as a result of death and tissue fixation.

In terms of facial features, the orbit was not drastically deformed from the sample population as it was not significantly different from the average in MCPH-SCKL (table 3 and figure 8). The dimensions of the orbit were significantly decreased by approximately 20% along the major and minor axes or roughly 8-10 mm indicating that while the microcephaly uniformly decreased the dimensions of the orbit, the decrease may significantly impact ocular function. The superior length of the zygomatic arch was significantly impacted which supports the morphology of a triangular face, potentially increasing the length due to pronounced cheekbones (table 3 and figure 9a,b). Lastly, the nasal cavity was also significantly decreased in dimensions by approximately 20%, but not uniformly introducing more elongation (table 3 & figure 10a,b). This could indicate that MCPH-SCKL effects different parts of the bones of the face more significantly than others, or effecting specific bones attributing to uneven distortions in facial morphology.

The mandible was perhaps the most deformed by MCPH-SCKL. Volumetrically, the mandible in MCPH-SCKL was significantly reduced, even

taking into account that the MCPH-SCKL patient had 15 teeth along the mandible while 4 out of 5 of the sample population specimens did not have any which would have increased the volume of the model, as would be expected in a patient displaying micrognathia (table 4 & figure 1). However, the distance between the mandibular angles and the distances between the condyles and the average distance of the angles to the mental protuberance were not uniform (table 4). This indicates that the mandibular condyles and the inferior-anterior portions of the mandible were more drastically effected than inferior-posterior aspects. Clinically, these features are relevant to determine the proper treatments, as surgical options might be required along with dental options to evaluate the placement of the temporomandibular joint ligament attachments to remediate jaw dysfunction.

Comparisons between the normal population and the MCPH-Seckel Syndrome specimen may be distorted from real anatomy due to the age differences. The normal population consisted of a varied population from 50 years old, while the MCPH-Seckel specimen was only 30. This difference may have lead to some fo the anatomical distortion demonstrated in these specimens. Bone density decreases as a result of aging, and muscles lose their ability to achieve the same lavel of tension on bone. This results in a diminishment of boney formations at attachment sites. This could mean that the results shown may have been more significant had they been recorded from a similarly aged population.

The exploration of anatomical variation, and pathological morphometrics are an important aspect in understanding the relationship between form and function. Without quantitative measurements of these topics diagnostic criterion fails. In addition, prognoses and treatment plans require an understanding of the effects of the pathology on both the injured organ or tissue as well as the surroundings. Shape changes are especially prone to effect other tissues which could reults in subsequent pathologies or injuries. The challenge of statistically significant samples of MCPH-SCKL is difficult to solve because of its rarity, however, future work in this field should utilize larger sample populations of effected individuals, as the current study only takes into account a single sample, and a larger population of cadaveric specimens that are nearer to the age of the MCPH-SCKL sample. We have found that computational morphometrics can be a useful tool to analyze sample population variability and to determine clinically relevant features of pathologies and their impacts on anatomical structures.

REFERENCES

[1] n.d. *3D Slicer.* Vers. 4.11.0. Brigham Women's Hospital, Harvard University. Accessed January 17, 2019. https://download.slicer.org.

[2] DeCoster, PJ, RM Verbeeck, V Holthaus, LC Martens, and A Vral. 2005. "Seckel syndrome associated with oligodontia, microdontia, enamel hypoplasia, delayed eruption, and dentin dysmineralization: a new variant?" *Journal of Oral Pathology & Medicine* 35 (10): 639-641.

[3] Fredorov, A, R Beichel, J Kalpathy-Cramer, J Finet, J-C Fillion-Robin, S Pujol, C Bauer, et al. 2012. "3D Slicer as an Image Computing Platform for the Quantitative Imaging Network." *Magnetic Resonance Imaging* 30 (9): 1323-1341.

[4] Hopkins, Timothy E, and Stephen J Haines. 2003. *Rapid development of Chiari I malformation in an infant.* Vol. 98. Journal of Neurosurgery.

[5] Joost, JM, Van Griethuysen, Andriy Federov, Chintan Parmar, Ahmed Hosny, Nicole Aucoin, Vivek Narayan, et al. 2017. *Radiomics.* Accessed January 22, 2019. http://www.radiomics.io/team.html.

[6] Kikinis, R, SD Pieper, and K Vosburgh. 2014. "3D Slicer: a platform for subject-specific image analysis, visualization, and clinical support." Edited by Ferenc A Jolesz. *Intraoperative Imaging Image-Guided Therapy* 3 (19): 277-289.

[7] Kjaer, Inger, N Hansen, KB Becktor, N Birkebaek, and T Balslev. 2001. "Craniofacial Morphology, Dentition, and Skeletal Maturity in Four Siblings with Seckel Syndrome." *Cleft Palate-Craniofacial Journal* 38 (6): 645-651.

[8] Majewski, F, and T Goecke. 1982. "Studies of microcephalic primordial dwarfism I: approach to delineation of the Seckel syndrome." *American Journal of Medical Genetics* 12 (1): 7-21.

[9] O'Driscoll, M, A R Grennery, J Seidel, P Concannon, and P A Jeggo. 2004. "An overview of three new disorders associated with genetic instability: LIG4 syndrome, RS-SCID and ATR-Seckel syndrome." *DNA Repair* 3: 1227-1235.

[10] O'Driscoll, Mark, Victor Ruiz-Perez, C. Geoffrey Woods, Penny A. Jeggo, and Judith A. Goodship. 2003. "A splicing mutation affecting expression of ataxia-telangiectasia and Rad3-related protein (ATR) results in Seckel syndrome." (Nature Genetics) 33 (4).

[11] Regen, A, LP Nelson, and SB Woo. 2010. "Dental manifestations associated with Seckel syndrome type II: a case report." *Pediatric Dent.* 34 (5): 445-450.

[12] 2015. *Seckel syndrome.* November 9. Accessed January 23, 2019.

[13] https://rarediseases.info.nih.gov/diseases/8562/seckel-syndrome.